F. Castro Cerda, C. Goulas, I. Sabirov, S. Papaefthymiou, A. Monsalve, R.H. Petrov. Microstructure, texture and mechanical properties in a low carbon steel after ultrafast heating. ***Materials Science and Engineering A***. Vol. 672, 2016, pp. 108-120.
DOI: http://dx.doi.org/10.1016/j.msea.2016.06.056

Microstructure, texture and mechanical properties in a low carbon steel after ultrafast heating

F. Castro Cerda[a,b1], C. Goulas[c], I. Sabirov[d], S. Papaefthymiou[e], A. Monsalve[b], R.H. Petrov[a,c]

[a] Department of Materials Science and Engineering, Ghent University, Technologiepark 903, 9052 Gent, Belgium.

[b] Department of Metallurgical Engineering, Universidad de Santiago de Chile, Av. Lib. Bdo. O´Higgins 3363, Estación Central, Santiago de Chile, Chile.

[c] Delft University of Technology, Department of Materials Science and Engineering, Mekelweg 2, 2628CD Delft, The Netherlands.

[d] IMDEA Materials Institute, Calle Eric Kandel 2, Getafe, 28906, Madrid, Spain

[e] National Technical University of Athens, School of Mining & Metallurgical Engineering, Division of Metallurgy and Materials, Laboratory of Physical Metallurgy, 9, Her. Polytechniou str., Zografos, GR-157 80, Athens, Hellas

felipemanuel.castrocerda@ugent.be

k.goulas@tudelft.nl

ilchat.sabirov@imdea.org

spapaef@metal.ntua.gr

alberto.monsalve@usach.cl

roumen.petrov@ugent.be

[1] Corresponding author. Tel.: +32 9 331 04 64; fax: +32 9 264 58 33
E-mail address: felipemanuel.castrocerda@ugent.be (F. Castro Cerda).

Abstract

Heating experiments in a wide range of heating rates from 10 to 1200 °C/s and subsequent quenching without isothermal soaking have been carried out on a low carbon steel. The thermal cycles were run on two different cold rolled microstructures, namely ferrite + pearlite and ferrite + martensite. It is shown that the average ferritic grain size, the ferrite grain size distribution, the phase volume fractions and the corresponding mechanical properties (ultimate tensile strength and ductility) after quenching are strongly influenced by the heating rates and the initial microstructure. The ferrite grain size distribution is significantly modified by the heating rate, showing a markedly bimodal distribution after fast annealing. The rise of the heating rate has produced a change in the relative intensities of texture components, favouring those of the cold-deformed structure (RD fibre) over the recrystallization components (ND fibre).

Keywords: ultrafast heating, steel, microstructure, texture, grain size, mechanical properties

1. Introduction

Steel industry is nowadays facing the challenge of producing materials with enhanced properties to meet the safety and fuel efficiency standards of the strict environmental and legal authority regulations (EU and USA) [1]. The development of Advanced High Strength Steels (AHSS) was a reaction of the steel industry to these societal needs [2]. The beneficial combination of enhanced strength and toughness was reached due to unique microstructures generated in this steel family. Lately, new processing routes, such as the quenching and partitioning (Q&P) and the ultra-fast heating (UFH) path, attempt to further improve Interstitial Free (IF), Dual Phase (DP), Transformation-induced plasticity (TRIP) and Martensitic steel (MS) grades. Additionally, the design of steels via UFH can deliver very high strengths due to the initiation of a mixed and/or synergetic bainitic/martensitic transformation. The aforementioned new thermal routes carried out in laboratory [3–6] or in small scale industrial conditions [7] have produced steels with superb mechanical properties, which evince the large but not yet used potential of the UFH treatments in steel manufacturing. The heating with very high heating rates is not a new practice in the heat treatment and it has found its place in the surface thermal treatment of the structural steels for general application, i.e. steels with carbon content of 0.35 to 0.6 %C (case hardening). However, its application to sheet materials and low carbon grades like AHSS has not yet been studied in details. In particular UFH stands out for its adaptability to the steel processing lines. Besides the improvement of the mechanical properties, UFH offers the opportunity of reducing the annealing steps for steel sheets and tube production. However, due to a number of technical difficulties of realization in large scale, UFH is not yet ready for industrial application in the existing continuous annealing lines.

The grain refinement effect of UFH on low carbon steel has been demonstrated [5,6,8–15]. Muljono et al. have reported a decrease in the recrystallized ferritic grain size after annealing cycles with heating rates up to 1000 °C/s [8]. The refining effect was also shown on IF steels [16], where the average ferritic grain (AFG) size was reduced to certain saturation point of 6 μm (at the heating rate of ~1000 °C/s), above which no further grain refining effect was observed. Such measurements were found to be consistent with later measurement of ferritic grain size versus heating rate in TRIP composition steels [6,9–12,14]. The much lower saturated AFG size measured (~1.5 μm) in the latter experiments in comparison to the one measured in IF steel suggests the interaction of the deformed ferrite with grains of second phase during recrystallization and phase transformation stages.

UFH influences not only the microstructure but the texture of the cold rolled steel [6,9–12,14,15,17]. In UFH treated cold rolled IF steel no general changes in the orientation components are observed when the recrystallization is finished before the onset of austenite formation [16]. The trends seem to be similar for low and very low carbon steels [17,18]. However, in cold rolled AHSS with initial microstructure of ferrite and pearlite after slow reheating (10 and 50 °C/s) the cold rolling texture changes to the crystallization type texture, which is characterized by a strong {111}⟨uvw⟩ (ND fibre) with specific curvature, and in which the RD fibre component {hkl}⟨110⟩ is almost vanished or quite weak. Contrarily, the texture of the cold rolled samples reheated at 1000 °C/s and 3000 °C/s remains almost unchanged even after reheating up to 880 °C keeping the characteristic features of the BCC cold rolling texture [6,9–11,14]. Petrov et al. [6,9,14] have rationalized the influence of UFH on the texture as an effect of the stabilization in the recovered structure of deformed ferrite by carbide precipitates and its contribution to the overall texture. Insignificant changes in rolling texture were reported also after UFH and quenching of steels with initial microstructure of cold rolled ferrite and martensite [10,12].

Analysis of the existing literature shows that very fine grained microstructures and correspondingly high ultimate tensile strength and elongation can be obtained in AHSS after employing fast and ultra-fast heating rates without isothermal soaking. The heating rates above 1000 °C/s allow recrystallization to be partially or completely suppressed and the crystallographic texture after UFH without isothermal soaking remains almost the same as the texture before the UFH treatment. On the other hand, the experiments in [6,9–11] clearly show that heating rates above 1500 °C/s do not contribute to grain refinement. However, the thermal treatment cycles reported in the literature are very difficult for practical implementation and the re-scaling to industrial conditions still remains a challenge, although the work of Cola et al. [7] shows that it is possible.

The aim on this work is to obtain a better understanding of the effect of heating rates and initial microstructure on phase transformations, recrystallization, texture and mechanical properties of a low carbon steel. To study the possibilities for an industrial implementation, all processing parameters are varied in a range which is considered as realistic for industry [15]. For the present study, the heating rates have been classified in the following ranges: conventional, (maximum of 10 °C/s), fast (from 10 to 100 °C/s) and ultrafast (higher than 100 °C/s).

2. Experimental

2.1 Material and heat treatments

The chemical composition of the studied steel is shown in Table 1. Steels with this composition are used as transformation induced plasticity (TRIP) assisted steel for automotive applications.

Table 1. Chemical composition of the studied steel.

C	Mn	Al	Si	Fe
0.19	1.61	1.06	0.50	Rest

The steel sheet of 1 mm thickness and a microstructure of ferrite and pearlite was received in condition after 50% cold rolling. Two sets of specimens with different initial microstructures were prepared from the selected steel. The first set of specimens denominated further as (50% F+P) set was kept in the as-received state, i.e. with the 50% cold deformation. The second set of samples (denominated as 50% M) was produced by annealing the initial steel sheet in the intercritical temperature range, where the microstructure consists of 50% ferrite and 50% austenite, and subsequently water quenched to produce a mixture of approximately 50% ferrite and 50% martensite. Next, the heat treated sheet was 50% cold rolled. Specimens of 80x25x1 (50% F+P) and 80x20x0.5 (50% M) mm^3 size were cut from each initial material and subject to different heat treatments, microstructural analyses and mechanical tests.

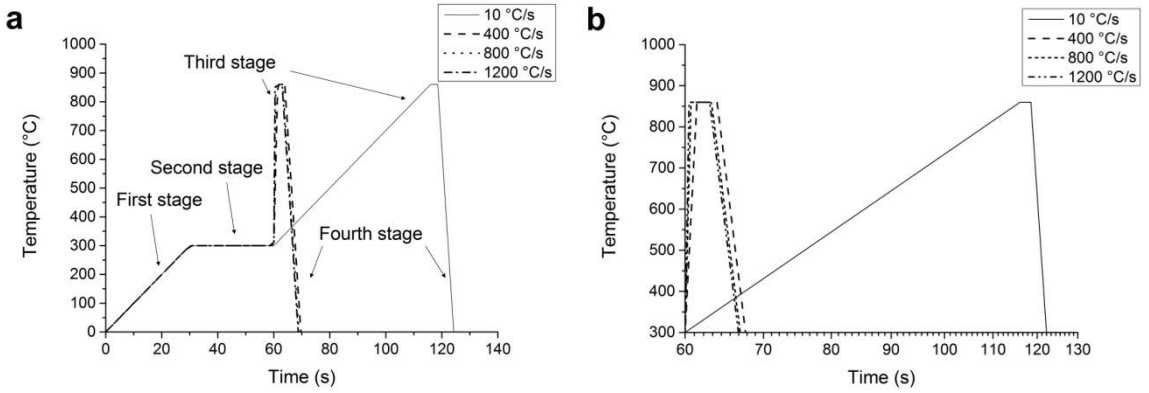

Fig. 1. Representation of the heat treatments: (a) the full thermal cycle and (b) the stages 3 and 4 for the different heating rates.

The phase transformation temperatures A_{C1} and A_{C3} of the steel were measured at a heating rate of 10 °C/s in the DIL805AD Bähr dilatometer. The measured critical temperatures were Ac_1^{10} = 728 °C and Ac_3^{10} = 923 °C. It was earlier reported that the transformation temperatures depend on the heating rate as well as on the initial microstructure [18]. Thus, the actual transformation temperatures for the heating rates above 10 °C/s will be different. Critical temperatures at heating rates of 400 °C/s and 1000 °C/s could not be measured by dilatometry with acceptable accuracy due to the instability of the system.

The specimens were subjected to different rapid heating cycles followed by subsequent water quenching. Motivated by the capacity of current continuous annealing lines [15], it was decided to study continuous heating cycles with two heating rates as shown in Fig. 1. Each thermal cycle contains 4 stages. On the first and second stage, the specimens were heated at 10 °C/s to 300 °C and next isothermally held at 300 °C for 30 s. These stages simulate a preheating stage in some industrial continuous annealing lines. On the third stage, the specimens were heated from 300 °C to 860 °C at four different heating rates, 10, 400, 800 and 1200 °C/s, and held at 860 °C for 1.5 s. The heating temperature was selected to be in the intercritical temperature range, where different fractions of ferrite and austenite are in equilibrium. The isothermal holding time was strictly controlled and never exceeded 1.5 s. Finally, the specimens were quenched from 860 °C to room temperature using Helium gas spray quenching and the cooling rate of ~-130 °C/s was achieved. This cooling rate is approximately 3 times higher than the critical cooling rate of ~-50 °C/s which is required to form pure martensitic structure in this steel. This approach allowed us to use martensitic structure as indication of the formation of austenite during the fast heating experiments. All heat treatments were carried out in a Gleeble 3800 thermo-mechanical simulator. The specimens are heated by the electrical current passing throughout the plate specimen and then quenched with a water spray. The temperature is controlled by means of a “K - type” thermocouple, spot welded to the midsection of each specimen. A homogeneous heat treated zone with a minimum length of 10 mm was produced in this way. The homogeneity of the temperature in this zone was controlled by 3 thermocouples and after the heat treatment was proved by hardness measurements and microstructural characterization along the sample length.

2.2 Microstructural characterization

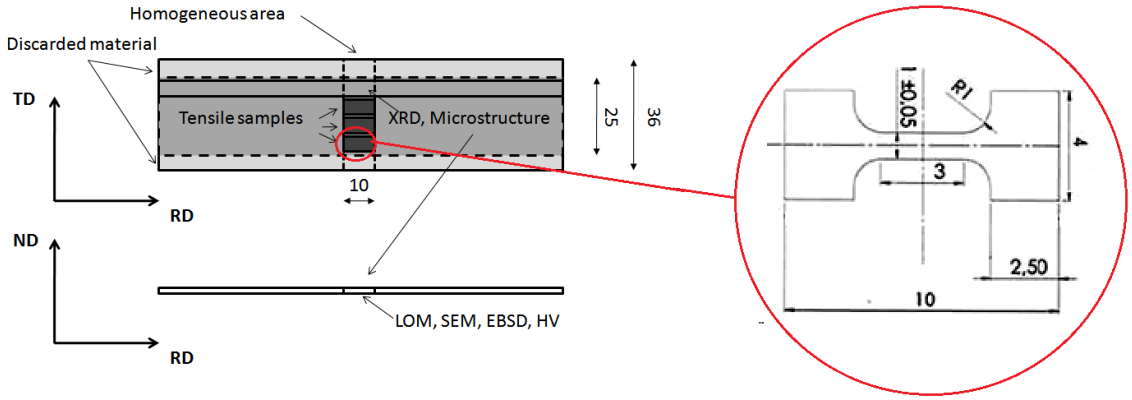

Fig. 2. Schematic representation of heat treated samples with the position and a drawing of the tensile sample.

Samples were cut from midsection of each heat treated specimen (as shown in Fig. 2) in order to characterize the microstructure and properties of the material in zone, which has undergone strictly controlled temperature-time cycle. For mechanical tests, 3 sub-size tensile samples were cut from

each heat treated specimen parallel to the rolling direction (RD). The gage length and width of the tensile samples are 3x1 mm^2, respectively. The microstructure evolution was followed by Optical (OM) and Scanning Electron Microscopy (SEM). Samples were prepared according to the standard procedure, i.e., by grinding and polishing to 1 μm diamond paste, and the microstructure was revealed by etching with solution of 4% HNO_3 in ethanol (Nital 4%) for ~10 s at room temperature. Electron backscatter diffraction (EBSD) analyses were performed on samples after grinding and polishing with final polishing step with 0.035μm colloidal silica for 40 min and polishing force of ~5 N. The EBSD patterns were acquired on FEI Quanta™ 450-FEG-SEMoperated at 20 kV, beam current corresponding to FEI spot size 5 for aperture 30 μm and working distance of 16 mm. The sample was 70° tilted towards the EBSD detector, and the EBSD patterns were acquired with a Hikari detector operated with EDAX-TSL-OIM-Data Collection V.6 software in hexagonal scan grid with step size of 50nm.

The orientation data were analysed using the following grain definition: misorientation higher than 5°, minimum 4 points per grain and points with a confident index (CI) lower than 0.1 were not considered in data analysis as dubious.

X-ray diffraction analysis was carried out using a Siemens D5000 diffractometer, equipped with Mo source (λ = 0.7107 Å). The angular range 2θ between 26°and 40° was scanned with a step size 0.03 °/step and time per step 20 s.

Vickers hardness (HV_3) was measured on each sample after thermal cycle and the hardness value was accepted as an average of at least five measurements per sample.

3. Results

3.1 Microstructure

Fig. 3 displays SEM images of the two sets of specimens with different initial microstructures after cold rolling (Fig. 3a, d), cold rolling followed by heating at 400 °C/s (Fig. 3b, e) and 1200 °C/s (Fig. 3c, f) to 860 °C and quenching. Typical cold rolled microstructures consisting of elongated grains of deformed ferrite and pearlite (Fig. 3a) or deformed ferrite and martensite (Fig. 3d) are observed. After the second stage of the annealing cycle (30 s isothermal holding at 300 °C), no significant changes in the morphology of the phases in F+P initial material were observed. However, in 50% cold rolled samples with mixed microstructure of ferrite and martensite the tempering of martensite takes place. This was noticed by the observation of the well-known structure of tempered martensite with cementite precipitates (Fig. 4a).

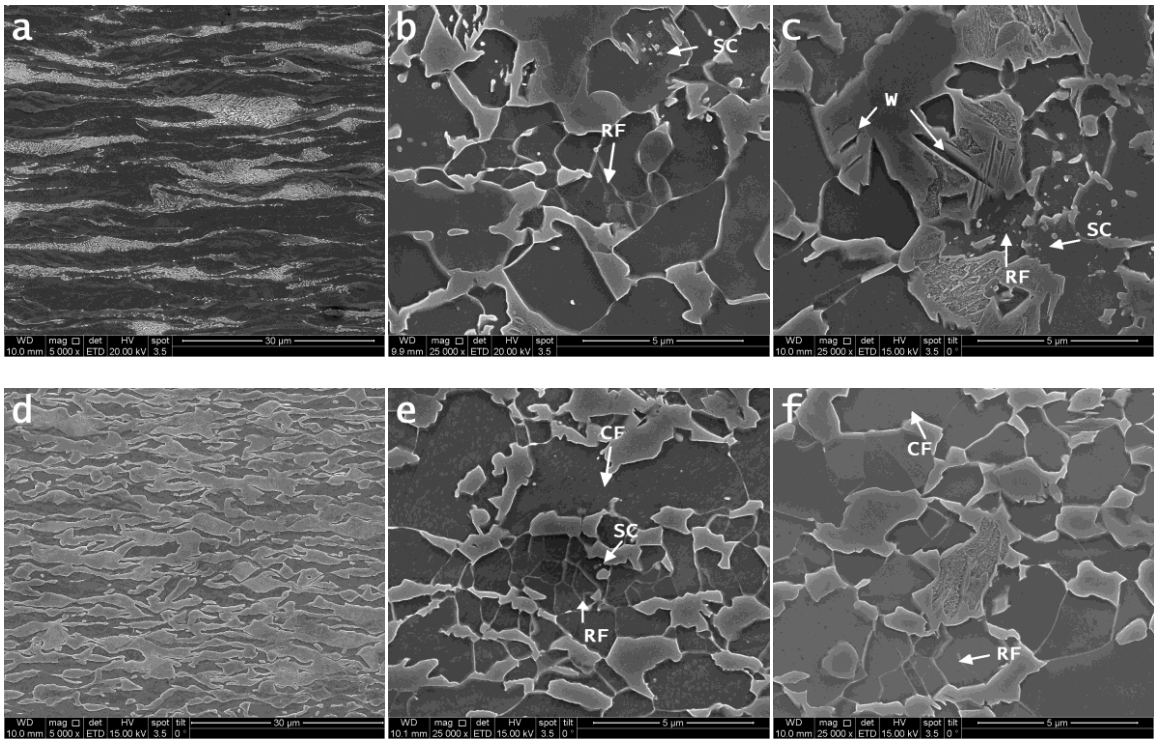

Fig. 3. SEM images of (a) 50% cold rolled F+P microstructure before heat treatment; (b), cold rolled F+P samples heated at 400 °C/s to 860 °C and quenched; (c) cold rolled F+P sample heated at 1200 °C/s to 860 °C and quenched; (d) samples 50% M microstructure after cold rolling, (e) after heating at 400 °C/s to 860 °C and quenching and (f) after heating at 1200 °C/s to 860 °C and quenching. All samples are etched with 4% Nital.

The microstructures after complete annealing treatments in all cases are mixtures of recovered ferrite (marked by arrows in Fig. 4) and/or recrystallized ferrite, newly formed martensite (light gray-white areas) and retained austenite. In all cases, different ferrite grain morphologies were observed. The ferrite phase in the microstructure is composed of large and small equiaxed ferrite grains. Different morphologies of Widmanstätten ferrite (W) were also observed, probably formed at the early stages of cooling. Fig. 4c - d shows ferrite plates of different types, according to Aaronson [19]. Notice that a mixture of upper and lower bainite (marked by arrows) is surrounding the ferrite plate in Fig. 4e.

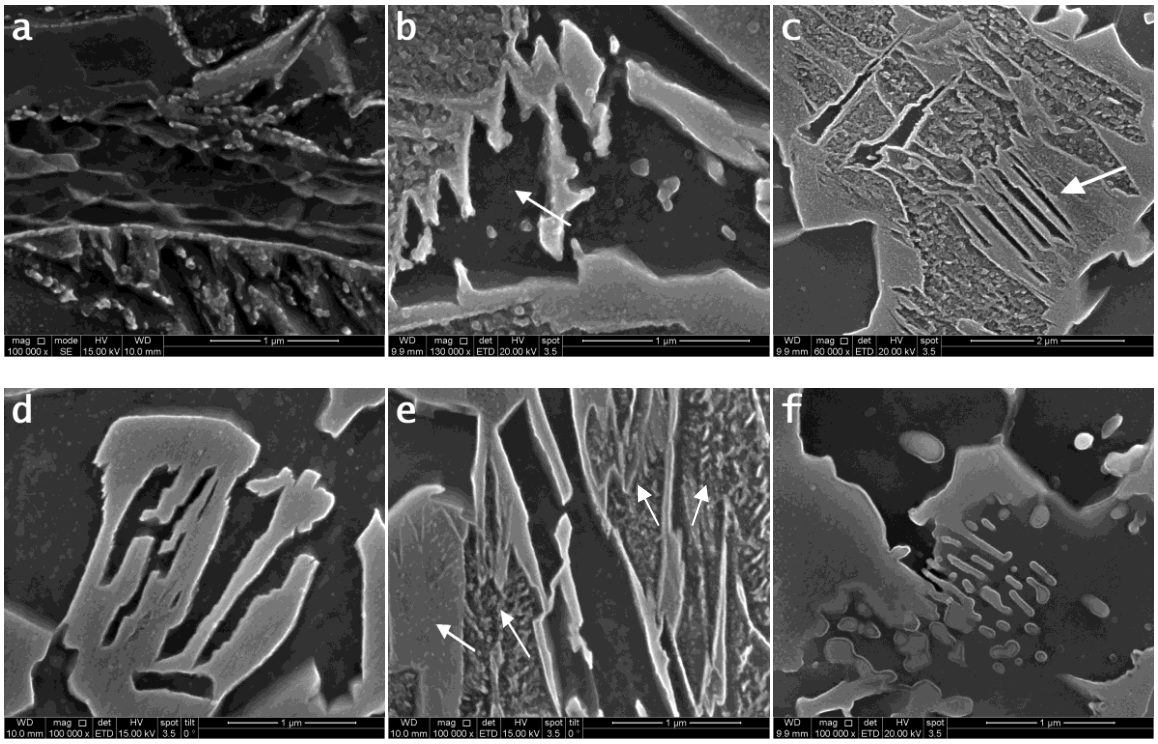

Fig. 4. (a) 50% cold rolled steel with ferrite-martensite microstructure, heated at 10 °C/s to 300 °C for 30s and quenched. Tempered martensite (upper and lower grains) and deformed ferrite (centre);(b) and (c) are 50% cold rolled steel with F+P microstructure heated at 400 °C/s to 860 °C and quenched. In (b), secondary 'sawteeth' and in (c) intragranular (lenticular) Widmanstätten ferrite plates are seen.(d) cold rolled 50% M microstructure, heated at 10 °C/s to 860 °C and quenched showing type B degenerated plates [19]. (e) 50% cold rolled steel with F+P microstructure heated at 1200 °C/s to 860 °C and quenched, degenerated Widmanstätten ferrite plate surrounded by upper and lower bainite (marked by arrows), (f) 50% cold rolled steel with F+P microstructure heated at 800 °C/s to 860 °C and quenched showing partially dissolved pearlite colony.

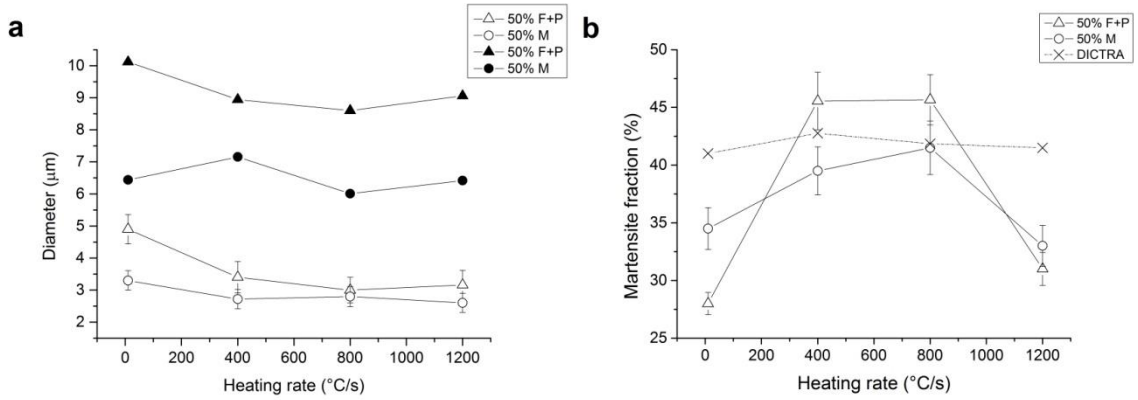

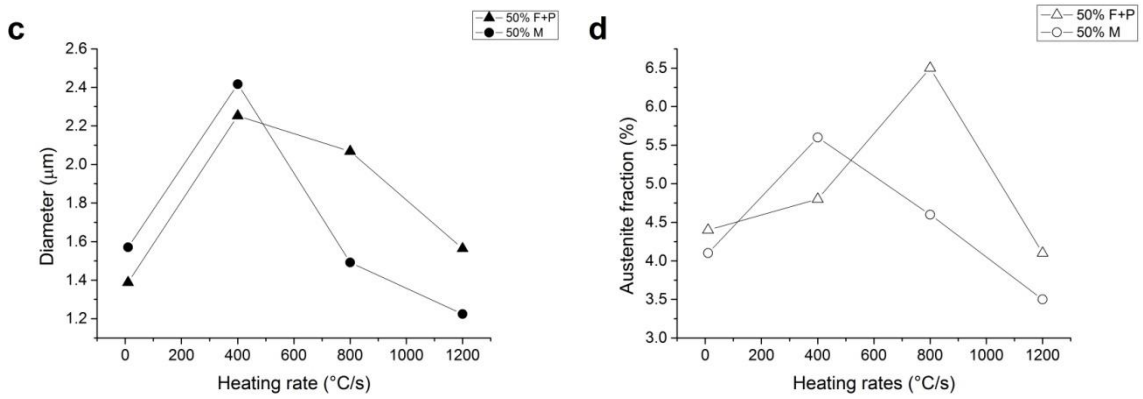

Fig. 5. (a) AFG size (lower set, outlined marks) and maximum ferritic grain size (upper set, filled marks), (b) Martensite phase fraction,(c) Maximum martensite grain size measured by EBSD and (d) retained austenite (RA) fraction versus heating rate. The annealing temperature and the holding time are 860 °C and 1.5 s, respectively.

As-quenched martensite is mainly distributed along bands and at grain corners (triple junctions) in both F+P samples and 50% M samples. Large martensitic blocks normally lock inside one or several plates of Widmanstätten ferrite. A part of the retained austenite grains is located inside the martensite blocks, and the other part within large ferrite grains or in grain triple junctions as spherical particles. Spheroidized cementite (SC) was observed in areas of unrecrystallized ferrite and inside martensite blocks. In 50% cold rolled F+P material heated at 800 °C/s, partial decomposition of the pearlite structure into austenite (transformed into martensite on cooling) was observed (Fig. 4f).

For further analysis of the microstructure the transformation products of the austenite formed during heating will be referred to as “martensite”, even though it is very clear that their microstructure is much more complex, as it was shown above. The resulting average ferritic grain (AFG) size is shown in Fig. 5a (lower set of curves). There is a noticeable decrease of the AFG size as the heating rate is raised up to 400 °C/s. The decrease of the AFG size with increasing heating rate is better pronounced in the steel with initial F+P microstructure. At heating rates of 400 °C/s and higher, the AFG size tends to reach a plateau, and the grain refining effect is negligible. The grain refining effect in the samples with 50% M is weaker than in the F+P samples in the same range of heating rates. The martensite grain size was also influenced by the heating rate.

The fractions of martensite at different heating rates are shown in Fig. 5b. The phase fractions are influenced by the heating rate in all cases, and the samples with 50% M initial microstructure display lower sensitivity of the martensite fraction to the heating rate in comparison to the F+P samples. Nonetheless, the shape of the two curves is similar, and they both show a risen the formed martensite fraction as the heating rate is increased up to 800 ^{o}C/s. At the heating rate of 1200 °C/s martensite fractions drop down, because the fraction of the transformed austenite during heating decreases due to the shift of the Ac_3 temperature towards higher values. A somewhat similar variation of the retained austenite (RA) fraction was measured. Cold rolled F+P initial microstructure

displays similar dependence of RA fraction on the heating rate, with an increasing tendency up to 800 °C/s and then an abrupt decrease (Fig. 5d). Similar tendency is observed in the samples with 50% M initial microstructure with the maximum RA fraction at 400 °C/s (Fig. 5d).

3.2 Texture

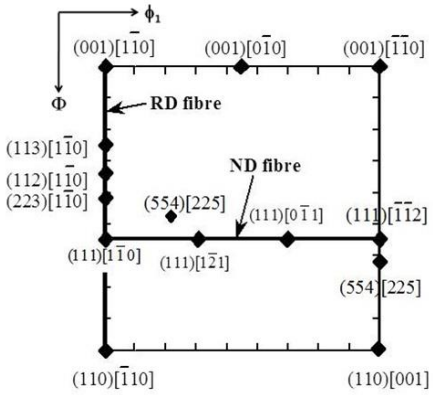

Fig. 6. Main BCC texture components shown in φ_2 = 45°section of the Euler space.

Fig. 6 shows the key for the main BCC texture components in φ_2 = 45° section of the Euler space. Fig.7 displays the calculated Orientation Distribution Functions (ODF) at φ_2 = 45° for ferrite in samples with both F+P and 50% M initial microstructures for heating rates of 10 °C/s and 1200 °C/s. The cold rolled samples with F+P initial microstructure (Fig. 7a,b,c) have noticeable texture variations with increasing heating rate, whereas 50% M samples (Fig. 7d,e,f) show weak texture intensities after all thermal cycles. The initial textures after cold rolling (Fig.7a,d) show alpha {uvw}⟨110⟩ and gamma {111}⟨uvw⟩ textures with pronounced maxima in the vicinity of the {111}⟨110⟩ components of ~6 mrd (multiples of random density) and weaker {112}⟨110⟩ with intensity of 2.7 mrd for the F+P samples. The texture of 50% M samples is represented mainly by gamma {111}⟨uvw⟩ fibre with maximum of 2.7 mrd in the vicinity of the {111}⟨112⟩ texture component. Both textures are similar and typical for low carbon steels after cold rolling. After the first stage of annealing (300 °C for 30 s) no significant variations in the texture morphology are observed, compared to the texture of the cold rolled steel. The minor variations in the texture intensities can be associated to the statistical variations of the data.

The texture of the 50% F+P samples heated at 10 °C/s shows components with maximum intensity on the gamma fibre {111}⟨uvw⟩ texture components of 2.7 mrd. This specific curved shape of the gamma fibre texture is associated with the recrystallization texture in mild steels [20]. As the heating rate is increased to 1200 °C/s, the texture is similar to the one after cold rolling with even similar intensities of the alpha {uvw}⟨110⟩ and gamma {111}⟨uvw⟩ fibres. Besides the change in the predominant components with the heating rate, the maximum intensity value also increases with increasing heating rate (Fig. 7d).

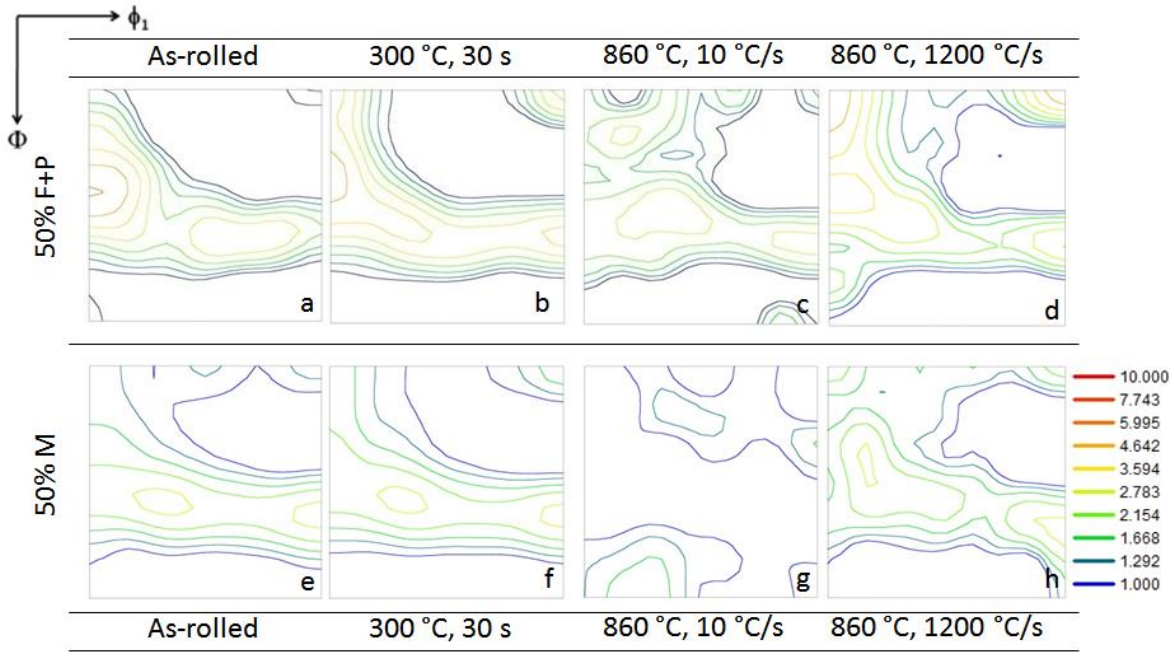

Fig. 7. ODFs at φ_2= 45° of ferrite in both samples after 50% cold rolling and heat treatment as follows: (a), (e)- initial texture after 50% cold rolling; (b) ,(f) -specimens held at 300 °C for 30 s then quenched, (c), (g)- heated at 10 °C/s to 300 °C and held for 30 s then heated at 10 °C/s to 860 °C held for 1.5 s and quenched and (d), (h)- specimens heated at 10 °C/s to 300 °C and held for 30 s then heated at 1200 °C/s to 860 °C for 1.5 s then quenched. (a), (b), (c) and (d) initial microstructure of ferrite and pearlite, (e), (f), (g) and (h) initial microstructure ferrite and 50% M.

Very similar effect of the heating rate on texture is observed in the samples with 50% M initial microstructure. Besides that the alpha–gamma-alpha phase transformation took place after reheating at 1200 °C/s to 860 °C and quenching, the texture (Fig. 7d, h) remains with similar morphology and intensity like after cold rolling or cold rolling and annealing at 300 °C for 30 s.

These observations are indication that after reheating with heating rates as high as 1200 °C/s the recrystallization of the cold rolled structure is strongly suppressed.

3.3 Tensile tests

The ultimate tensile strength (UTS) and elongation to fracture were determined in all heat treated specimens, and the data is shown in Fig. 8. In all materials, the UTS increases with increasing heating rate up to 800 °C/s, then it drops. As with the hardness measurements, the highest values of UTS were measured in 50% M samples. In this case, the sensitivity of the UTS to the heating rate is higher for the range between 10 °C/s and 400 °C/s for 50% M samples, in comparison to the F+P samples. The 50% M samples show an increment of ~200 MPa from 10 to 800 °C/s heating rate. The final elongation also shows a marked increment between 10 and 400 °C/s, similar to the UTS values. Above 400 °C/s, the elongation to fracture is in the range between ~25% and ~30% for 50% F+P, and

between ~16% and ~22% for 50% M material. 50% F + P material shows higher ductility than 50% M for all heating rates.

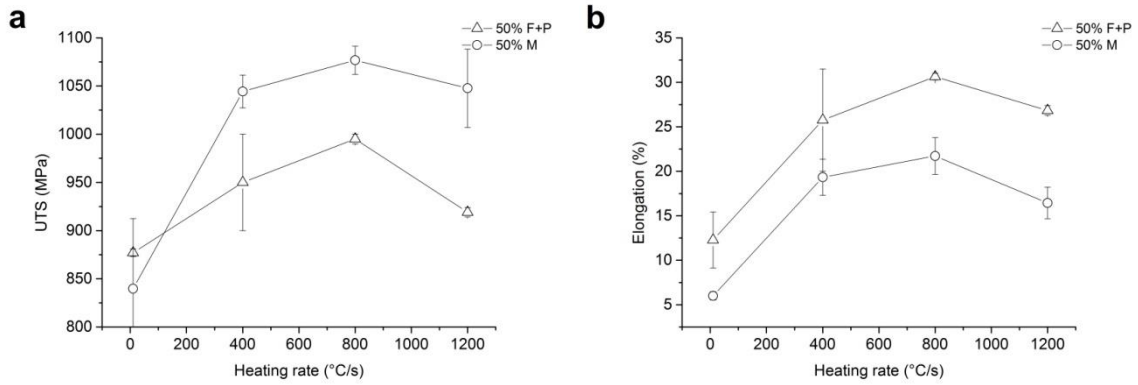

Fig. 8. (a) UTS values and (b) elongation to fracture versus heating rate. The annealing temperature and the holding time are 860 °C and 1.5 s, respectively.

4. Discussion

4.1 Ferrite recrystallization and growth

In order to distinguish ferrite from martensite, average EBSD image quality (IQ) maps were used to assess both phases. Recrystallized ferrite normally produces high IQ patterns, whereas martensite produces lower quality patterns. Fig. 9c shows the histogram obtained from the plot of average IQ versus the area fraction of the grains. The phase identification was thus straightforward, since the microstructure after has a bimodal distribution. The data was subsequently divided in high average IQ data (red bars), which corresponds to ferrite, and low average IQ data (green bars) corresponding to martensite. Calculations of the average grain size and texture were, therefore, carried out in each phase separately.

A relatively uniform distribution of equiaxed grains of ferrite was observed in material heated at 10 °C/s. However, as the heating rate is increased, large isolated elongated grains seem to stand out from the matrix. The formation of such large grains influences the histograms of grain size distribution shown in Fig. 10. Blue curves represent material heated at 10 °C/s, whilst red curves represent material heated at 1200 °C/s. It can be readily noticed that the increase in the heating rate shifts average grain size towards lower values. Nevertheless, the most remarkable feature in red curves is the change in the shape of the histogram. At first glance, blue curves have 2 peaks, one small at around 2,5 μm and another at larger grain size. Red curves show that, after UFH at 1200 °C/s, the first peak grows in intensity with respect to the second peak. This means that the fraction of finer grains has increased, whereas the second peak is still noticeable in all red curves. The grains that recrystallized first during heating and had more time to grow are larger and

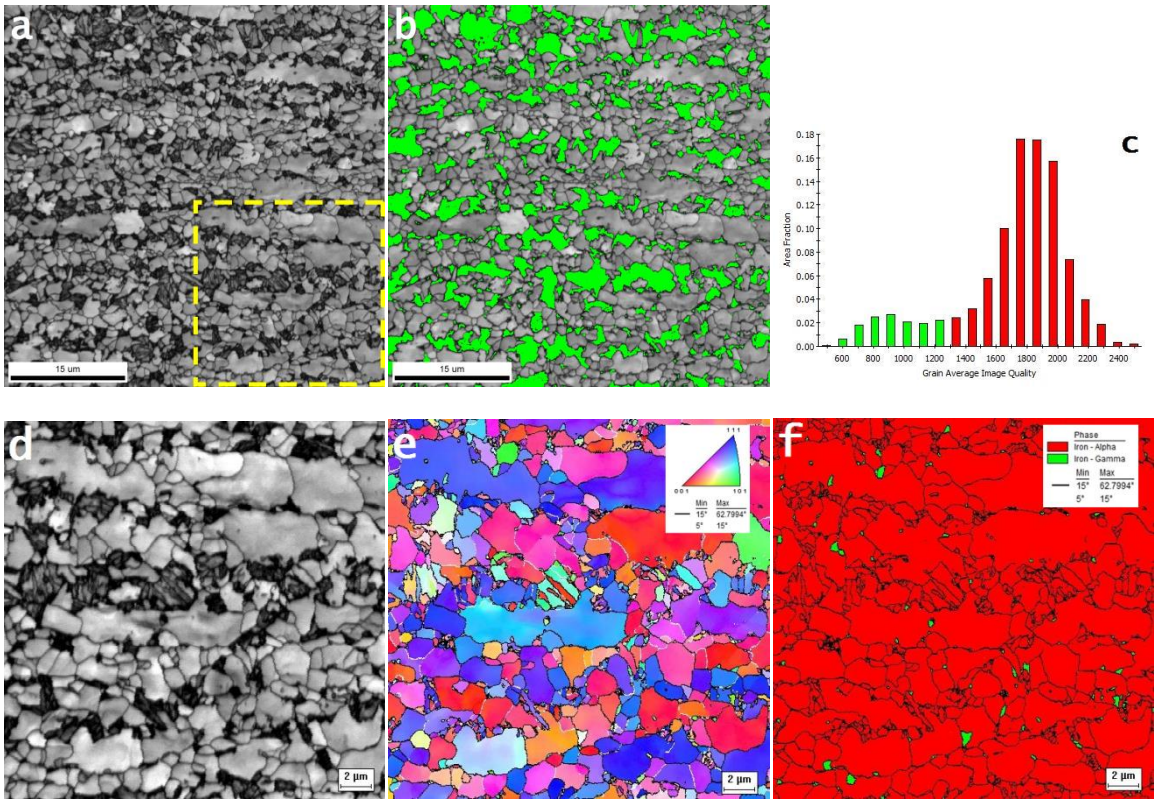

Fig. 9. EBSD scan of 50% F+P material heated at 400 °C/s. (a) IQ map, (b) IQ map with low average IQ grains (martensite) highlighted, (c) plot of the average IQ versus area fraction of grains, (d) selected area of the IQ map in (a), (e) inverse pole figure (IPF) and (f) phase map of the selected area. Step size 50 nm.

represented by part of the curve that contains the second peak. EBSD data clearly shows that these first recrystallized grains have grown by the mechanism of coalescence [20,21].

Evidence of the coalescence of ferrite grains is shown in Fig. 9e. The misorientation angles (MA) between 15 and 63° are marked by black lines, whereas the MA between 5 and 15° are outlined in white. Arrows in the Inverse Pole Figure (IPF) map show grains with similar orientation, although some small variations within the grains are noticeable. Such variations are in all cases lower than 5°. The large elongated grains have grown by the coalescence of smaller grains. The grains that seem to fast coalesce into large aggregates have, in most cases, MA below 15°. Grain boundaries with MA greater than 15° (HAGBs) seems not to be preferred to coalesce into large ones. Thus, the growth of fast coalesced grains will produce grain morphologies of irregular shape which, in most cases, is different from morphology of the equiaxed ferritic grain. Nonetheless, such morphologies can be easily rationalized assuming the coalescence mechanism. Similar, coalesced grain structure can be observed in all micrographs of fast annealed experiments in Fig. 3 (CF), although not as evident as in EBSD maps. In some cases, large single coalesced ferrite grains contain RA or martensite grains inside, as marked by yellow arrows in Fig. 9f. It is believed that, during heating, small pearlite colonies are trapped as result of the coalescence of ferrite grains. After the temperature of

transformation is reached, austenite is formed and it is retained or transformed to martensite during further quenching.

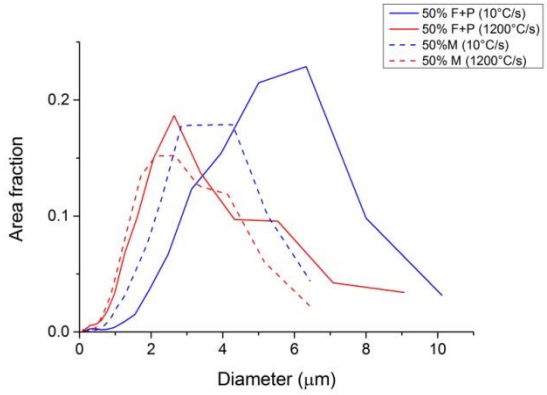

Fig. 10. Plot of grain diameter versus area fraction of grains. Data obtained from EBSD measurements. Solid and dashed lines represent 50% F+P and 50% M, respectively.

Although the amount of cold deformation apparently influences the maximum size of recrystallized ferrite grains (Fig. 5a), once it reaches a saturation heating rate (around 400 °C/s), it does not seem to be strongly affected by the heating rate. Considering that the largest grains are probably the first ones to recrystallize, it is possible to state that heating rate has either a narrow effect on the kinetics of recrystallization or that larger grains grow noticeably fast (irrespective of heating rate) until they impinge some sort of barrier that hinders further advance of the interface. It is well known that heating rate has actually an influence on the recrystallization starting temperature (T_R) [8,16,22,23] and on the recrystallization kinetics [8,23,24]. In spite of that, the current experiments are not conclusive regarding such parameters of ferrite recrystallization. It is believed that the size of the largest recrystallized grains is influenced primarily by the phase distribution in the initial microstructure. Moreover, it has been acknowledged that fine particles can act as barriers for the migration of grain boundaries [20,25]. Such interaction can take place during the tempering of martensite, and might as well explain the flat size profile measured in 50% M initial microstructure samples (Fig. 5a).

A modification of the recrystallization response of the material is certainly triggered by UFH. This statement becomes even more evident after establishing that the size of larger ferritic grains are slightly affected by the heating rate, particularly in 50% M initial microstructure. Previous experiments on the same steel with 50% F+P microstructure have revealed a decrease in the recrystallized fraction with increasing heating rate [11]. The most significant contribution to the grain refinement, therefore, lies in the grains that have 'recovered' structure and the grains that have recrystallized later, at higher temperatures. Areas of recovered structure were observed in all samples treated above 10 °C/s. These areas are characterized by groups of small grains (having size less than 1 μm), as indicated by white arrows in Fig. 4. It is believed that such areas correspond to recovered ferrite for two reasons that stem on EBSD data. Firstly, because of the presence of low angle grain boundaries; and secondly, EBSD data of these zones have revealed IQ values comparable

with those of recrystallized grains. Recovered grains should not be misled with large coalesced grains (marked by arrows in Fig. 9e).

4.2 Texture after UFH

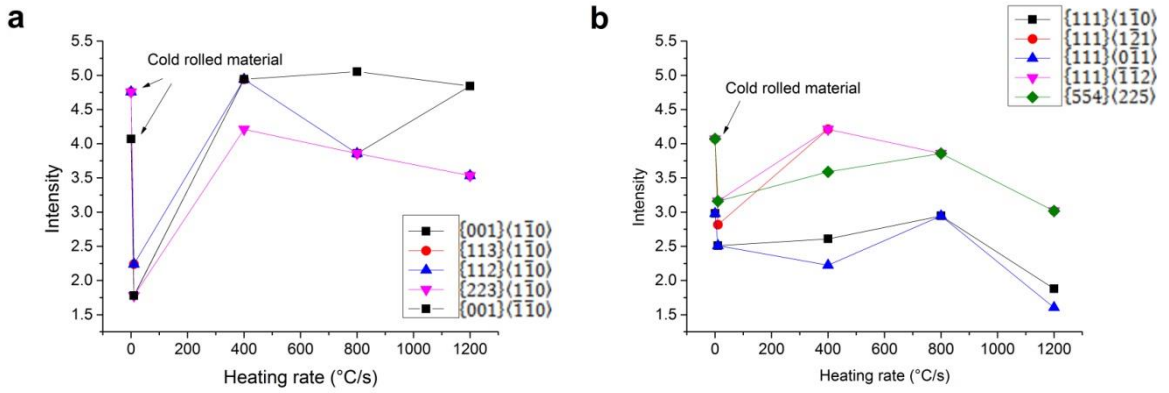

Fig. 11. Intensities of selected orientation components of 50% F+P initial microstructure in RD fibre (a) and ND fibre (b) versus heating rate.

The texture intensity in 50% M samples is very weak, as it was also reported in early works [6,10–12]. However, a slight increase in the maximum intensity of components of ND-fibre was measured as the heating rate is raised. The most noticeable features were, however, measured in samples with 50% F+P initial microstructure. Texture components are in fair agreement with previous results on TRIP composition steels [6,9–11]. The orientations observed after the second stage of the annealing cycle (30 s at 300 °C, Fig. 5b and f) suggest that recrystallization has not yet been activated. Only recovery has taken place at that stage. Although it has been established that the heating rate does not affect significantly the recrystallization textures in low carbon and IF steels below A_3 [16,17,26], it seems that this might not be true for TRIP composition steel. Fig. 11a shows the evolution of some components of alpha and gamma fibre in 50% F+P initial material. At lower heating rates, ND fibre components have slightly higher intensities than the components of alpha fibre. As the heating rate is increased, alpha fibre components are growing in intensity whilst ND fibre grains display a relatively constant intensity. At 1200 °C/s, ND fibre components have decreased intensities. It is well accepted that alpha fibre store less deformation energy than gamma fibre components [27–29], thus having less driving force for recrystallization. At lower heating rates, such low stored energy grains are consumed by recrystallized ND fibre grains which may have growth advantage (first nucleate – first grow). However, high heating rates could trigger the conditions for these RD fibre grains to reach the onset or recrystallization [22,23]. It is also reasonable to expect that a fraction of low stored energy grains will only activate the recovery, which contributes to the raise in the intensity of RD fibre components. Examples of recrystallized and recovered RD fibre grains can be observed in Fig. 9e (red grains). In consequence, recrystallization and growth of RD fibre grains might occur at higher temperatures, compared with most favourable ND fibre grains, and hence increasing the intensity of RD fibre components.

Notice that the change in the ferrite grain size distribution (Fig. 10) can serve as an indirect evidence of the change in the recrystallization behaviour described in the former section. At lower heating rates, the early recrystallized ND fibre grains (second peak from left to right) will grow at the expense of RD grains and therefore produce larger AFG. As the heating rate increases, the fraction of smaller grains (first peak) becomes much more significant, since the RD fibre grains with low stored energy are either able to reach the onset or recrystallization and thus nucleate new ferrite grains or rearranged into recovered low misorientation angle subgrain structure.

Widmanstätten ferrite grains also contribute to the overall ferrite texture. Nevertheless, its volume fraction is too low to have a significant contribution to the texture. The predominant orientation component in RA in all cases was the brass component $(110)[1\bar{1}2]$. A faint copper component $(112)[11\bar{1}]$ was measured with a maximum of around 1/6 of the intensity of the brass component. Both match the typical orientations of deformed austenite [30]. At the intercritical region, the transformation of austenite can only take place at the ferrite/cementite interface. Therefore, the orientation of ferrite-cementite aggregates that are retained to intercritical temperatures will determine the orientation of RA.

4.3 Austenite transformation

According to equilibrium calculations, the relative volume fraction of austenite at 860 °C is 60%. The measured phase volume fractions are thus close to the equilibrium value, in spite of the short annealing time. UFH experiments have produced curves of austenite formation with a maximum of austenite volume fraction at intermediate heating rates, as shown in Fig. 5b. Similar shape in martensite fraction versus heating rate has been measured at 825 °C [11].

In order to evaluate the contribution of the heating rate to the kinetics of austenite formation, calculations with the Dictra software were performed. The software solves the one-dimensional moving boundary problem by calculation of local equilibrium conditions in each time step. It was assumed an initial volume of radius equal to 2.5 μm (in accordance with the maximum martensite grain size measured by EBSD, Fig.5c). Only the heating and the holding stages at the intercritical range (stages 2 and 3, respectively) were simulated. The dissolution of cementite was assumed to be complete at 724 °C. The initial fraction of austenite was calculated with ThermoCalc (database TCFE6). The value was then corrected assuming that carbon does not contribute to the volume change in the system. Corrected volume fractions correspond to a value close to the initial pearlite fraction in 50% F+P microstructure. The quenching stage was not considered in the calculations. The results are shown in Fig. 5b (semi dotted-dashed line).

The calculated variation of the austenite fraction was virtually unaffected by the heating rate. The simulated curve seems to fit slightly better the 50% M initial microstructure, probably because the assumption of fully dissolved cementite is more appropriately approached by a finer cementite distribution product of the tempering of martensite. The deviations observed at low and high heating rates are therefore likely to be related with the variables that were not taken into account

in the simulations, such as nucleation rate, cementite coarsening and transformation of ferrite during cooling, as demonstrated in Fig. 3 and Fig. 4. The largest austenite grains are probably the ones that nucleated first, and thus had the longest time for growth. Consequently, if the kinetics of transformation is calculated after the overall reaction time, the results should fit better the maximum grain size, instead the average value, for instance. Such approach has been previously applied to the calculation of the plate growth kinetics of Widmanstätten ferrite and bainite in carbon steel [31]. The maximum martensite packet size is normally of a length comparable to the diameter of the parent austenite grain. It seems, thus, reasonable to relate the intercritical austenite growth kinetics to the largest martensitic grain, as shown in Fig. 5c. In the range from 400 to 1200 °C/s, a decreasing tendency is observed. This might be caused mainly by the delayed austenite nucleation, or the so-called 'shifting' of the intercritical curves triggered by the heating rates. Previous experiments [32] have shown that, when the transformation starts from initial martensitic structure, the effect is less pronounced. One could estimate the effect of the heating rate in the carbon gradient in austenite for anisothermal (peak annealing) experiments in the intercritical (α+γ) region with known parameters. The following analysis is only valid for austenite on heating and/or soaking. For simplicity, the sharp interface model is accepted and capillarity effects and volume changes associated to transformation shall be excluded. Let us define the final carbon gradient in austenite as

$$\frac{\Delta X}{\Delta y} = \frac{X_C^{\theta/\gamma} - X_C^{\gamma/\alpha}}{\Delta L} \quad (1)$$

where $\Delta X/\Delta y$ is the carbon gradient for the isothermal formation of austenite at some temperature within the intercritical (α+γ) region, $X_C^{\theta/\gamma}$ is the carbon content (mole fraction) of austenite in equilibrium with cementite, $X_C^{\gamma/\alpha}$ is the carbon content (mole fraction) of austenite in equilibrium with ferrite and ΔL is the width of the austenite grain. The radius of the austenite grain will be defined by some average velocity $\bar{v}$ of the interface during the time interval Δt

$$\bar{v} = \frac{\Delta L}{\Delta t} \quad (2)$$

The velocity of the austenite-ferrite interface shall be determined by the mobility of the austenite-ferrite interface and the chemical driving force for the growth stage, as defined elsewhere [33]. Solving for ΔL

$$\Delta L = \Delta t \cdot \bar{v} \quad (3)$$

and replacing in (1)

$$\frac{\Delta X}{\Delta y} = \frac{X_C^{\theta/\gamma} - X_C^{\gamma/\alpha}}{\Delta t \cdot \bar{v}} \quad (4)$$

in the case of anisothermal transformation under constant heating rate, the following definition can be made

$$\beta = \frac{\Delta T}{\Delta t} \quad (5)$$

where β is the constant heating rate and ΔT is the temperature range of the onset to the stop austenite formation. For the case of the present experiments,

$$\Delta T = T_P - A_{C1} \quad (6)$$

being T_P the peak temperature (860 °C) and A_{C1} the onset of austenite formation. Eq. (4) can thus be expressed as

$$\frac{\Delta X}{\Delta y} = \frac{\beta\left(X_C^{\theta/\gamma} - X_C^{\gamma/\alpha}\right)}{(T_P - A_{C1}) \cdot \bar{v}} \quad (7)$$

It´s interesting to note that, assuming $\bar{v}$ as constant in the entire temperature range defined in Eq. (6), Eq. (7) predicts a value of ΔL depending on the factor $(T_P - A_{C1})/\beta$. A_{C1} is known to increase with β [18,32], thus, a steeper effect can be predicted. A simple linear relation between the equilibrium temperature A_1 and A_{C1} could predict the variation shown by the dashed line in Fig 5c, which is decreasing over the UFH region, in agreement with the measured variation of maximum martensitic grain size with heating rate for both initial microstructures. The calculated diameters in Fig 5c (dashed line) were computed with the maximum interface velocity obtained with DICTRA (Fig. 12a). The value of $\bar{v}$ might as well be estimated numerically from Fig. 12a, assuming that

$$\bar{v} = \frac{1}{(t_f - t_i)} \int_{t_i}^{t_f} v \cdot dt \quad (8)$$

where t_i and t_f represent the onset and the finishing of the austenite formation and v is the instantaneous velocity of the γ–α interface. The calculated carbon gradient is shown in Fig 12b.

The modification in the cementite structure is also playing a role in the lower maximum diameter values and phase fractions of martensite at 10 °C/s. In F+P initial material, it was found that the cementite lamellas were almost fully spheroidized after 10 °C/s. It has been stated [34,35] that the nucleation of austenite in spheroidized microstructures takes place at the sites where the cementite is in contact with grain boundaries between two adjacent ferrite grains. Thus, not all the cementite/ferrite boundaries will serve as an active nucleation site for austenite. It is reasonable to expect that recrystallized and spheroidized structure, as in samples of both initial materials heated at 10 °C/s to 860 °C, will have less potential nucleation sites for austenite than partially deformed F+P microstructure in specimens treated at higher heating rates. The reduced number of active nucleation sites will substantially reduce the diameter and fraction of transformed austenite. For this reason, is Eq. 7 is unable to predict the actual variation of austenite diameter in the range of conventional heating rates (below 10 °C/s). At higher heating rates (above 400 °C/s, Fig. 4f), the pearlitic structure was virtually not modified before reaching the intercritical range, hence the available pearlite/pearlite and pearlite/ferrite boundaries for austenite nucleation was kept

constant and, thus, the main factor affecting the diameter and austenite phase fraction is the heating rate, as previously described. In 50% M initial microstructure samples, the Ostwald ripening of tempered carbides at lower heating rates may be producing an effect similar to spheroidized cementite in 50% F+P initial microstructure. At heating rates above 400 °C/s, the heating rate plays the most important role.

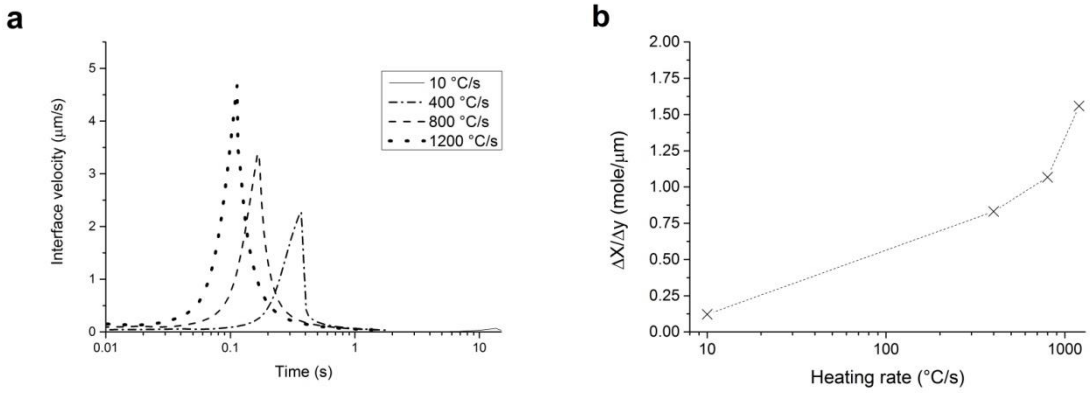

Fig. 12. (a) DICTRA simulations if the velocities of the γ–α interface versus temperature at different heating rates and (b) carbon gradient versus heating rate, as calculated from Eq. (7) and Eq. (8) assuming $A_{C1} = A_1 + p\beta$, with $p = 0.01s$. The other parameters used where $X_C^{\theta/\gamma} - X_C^{\gamma/\alpha} = 0.038$, $T_P = 860\,°C$ and $A_1 = 730\,°C$. All thermodynamic parameters where calculated using ThermoCalc software, database TCFE6.

Eq. (7) describes the influence of heating rate on the gradient of carbon produced in austenite after peak annealing. It is clear that for heating rates infinitely low, carbon gradients should be inexistent due to the factor β. The carbon gradient is expected to grow for high heating rates until, $(T_P - A_{C1}) = 0$, which determines the maximum carbon gradient. Above this limit, the transformation has not taken place. Hence, carbon gradient can be reasonably expected in peak annealing experiments after certain intermediate heating rate, as shown by Fig. 12b, and it should become steeper as the heating rate is increased.

Cementite dissolution was incomplete after all thermal cycles. This is also indirectly confirmed by the calculated carbon content in austenite by XRD. In all cases, a consistent value of ~1.1 %C was estimated [36]. According to calculations with Thermo-Calc, the carbon content of austenite in equilibrium with cementite at 860 °C is 1.19 %C.

4.4 Mechanical properties

Results of tensile test show that the UTS of the material after UFH cycles is primarily influenced by the phase fraction of ferrite and then by the ferritic grain size. The general shape of the variation of the UTS with the heating rate (Fig. 8a) is largely similar to the martensite fraction (Fig. 5b). The highest UTS values were recorded for 50% M initial microstructure, which shows the finest average

ferritic grain size. 50% F+P microstructure has in most of the points approximately 50 MPa lower strength than 50% M microstructure. Such values are also consistent with the hardness measurements. In 50% M samples, a relatively flat AFG and martensite fraction variation with the heating rate may satisfactorily explain the variations in UTS. 50% F+P samples have more significant variations in AFG size and the martensite fraction, and the strength is lower at most of the heating rates.

The variations of the elongation at fracture with the heating rate display a tendency similar to the variations in UTS values. However, 50% F+P material shows higher ductility than 50% M, consistent with the higher UTS values of 50% M samples shown in Fig. 8a. Analysis of fracture surfaces has shown that the ductility of martensite is playing an important role in the overall deformation behaviour of the tensile specimens. Each picture in Fig. 13 illustrates, on the left hand side, the fracture surface of tensile specimens and, on the right hand side, the microstructure corresponding to 50% F+P (13a, 13b and 13c) and 50% M (13d, 13e and 13f) after different thermal cycles. Figs 13a and 13d, which correspond respectively to 50% F+P and 50% M treated at 10 °C/s, clearly show areas that accumulates large and small amount of plastic deformation during the fracture process. By comparison between left and right hand sides on the aforementioned images, one can conclude that the areas that are heavily deformed correspond to ferrite and the rest are martensite. Figs. 13b, 13c, 13e and 13f, which correspond to heating rates of 800 °C/s (Figs. 13b and 13e) and 1200 °C/s (13c and 13f), are showing a more homogeneous distribution of strain in the microstructure. By analogy, this indicates that the martensite (or the martensite-bainite aggregates) are withstanding higher strain levels, compared to martensite aggregates in material of both initial conditions heated at 10 °C/s. In contrast, the fraction of ferrite is lower at heating rates above 10 °C/s, as indirectly displayed in Fig. 5c. Therefore, the amount of strain that the other constituents (martensite, bainite, retained austenite) undergo becomes more significant during necking and fracture.

It is reasonable to state that heterogeneous nature of the microstructure after UFH has a noticeable impact on the mechanical properties. This has been shown in other systems as well [37,38]. The specific deformation behaviour of the martensite-bainite aggregates is consequence of the composition and morphology of the austenite. As shown in Fig. 12b, carbon gradients can be reasonably expected in UFH experiments. It is, thus, also reasonable to conclude that the heating rate has a noticeable effect on the strength and ductility. Additional microstructural constituent like retained austenite (and a subsequent TRIP effect) could also play a role in the variation of the strength and ductility [39–41]. Furthermore, the unique microstructural features resulting from UFH, such as the described carbon gradients in austenite and partial restoration processes [3,28,29], significantly affect the mechanical properties of the material.

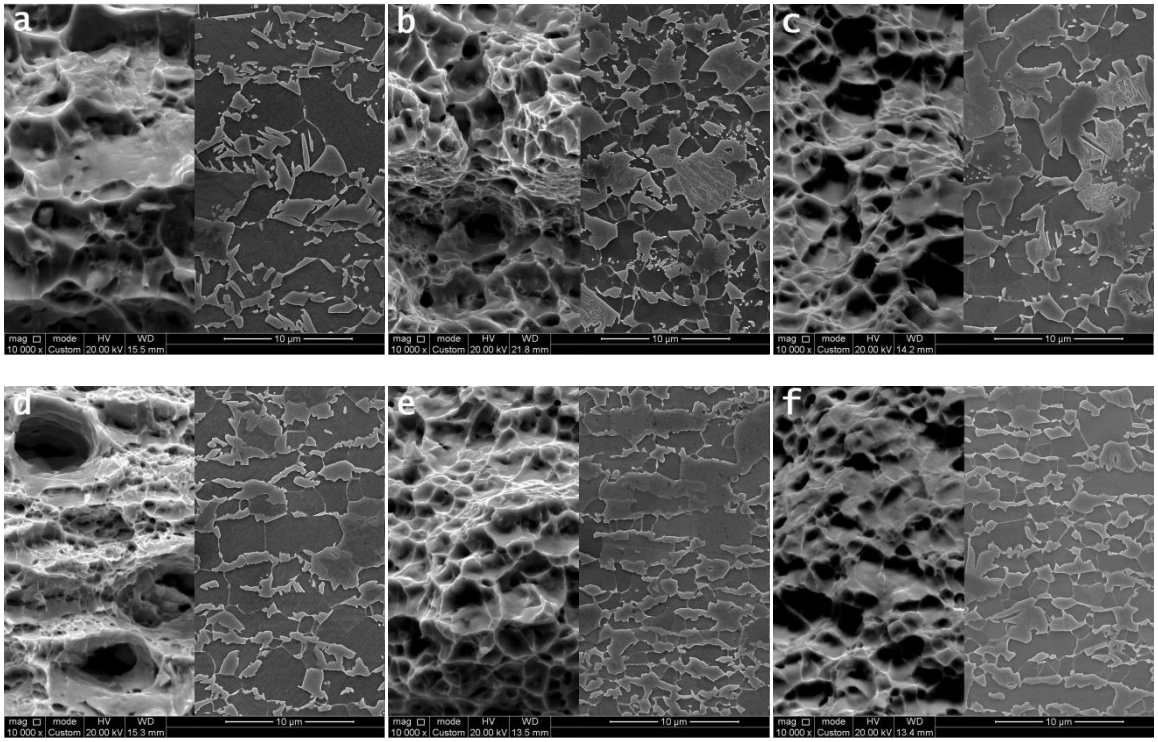

Fig. 13. Fracture surface of the material after tensile test. (a), (b), (c) correspond to 50% F+P and (d), (e), (f) correspond to 50% M initial microstructure, respectively. (a) and (d), (b) and (e), and (c) and (f) correspond to samples heated at 10 °C/s, 800 °C/s and 1200 °C/s, respectively. In each image, the right hand side half corresponds to the microstructure before tensile test.

5. Conclusions

Heating experiments in a wide heating rate range (10 - 1200 ^{o}C/s) were carried out on an Fe-0.2C-1.6Mn-1.06Al steel with two different initial microstructures and the results are summarised as follows:

The kinetics of ferrite to austenite transformation in the intercritical range is strongly influenced by the heating rate. It was shown that, in anisothermal (peak annealing) experiments, carbon gradients in austenite are to be expected above certain heating rate and will become steeper as the heating is increased up to a defined limit. Carbon gradients are playing a major role in the mechanical properties of the studied steels.

Thermal cycles under different heating rates produced a bimodal distribution of the ferritic grain size. The appearance of the bimodal grain size distribution depends on the initial microstructure and the recovery and recrystallization processes during ultra-fast heating.

It was confirmed that UFH significantly contributes to the grain refinement when heating rates above 10 °C/s are applied. The effect of UFH in the decrease of ferritic grain size is more pronounced in ferrite and pearlite initial microstructure.

Increasing heating rate strongly affects the relative intensities of texture components, favouring those of the cold deformed structure (RD fibre) over the recrystallization components (ND fibre). This is an indication that after reheating with heating rates as high as 1200 °C/s the recrystallization of the cold rolled structure is suppressed.

The subsequent increase in the heating rate has produced an improvement in both strength and ductility at heating rates up to 800 °C/s ; when heating rates are 1200 ^{o}C/s, the UTS and elongation at fracture decrease. Such behaviour is primarily associated with the carbon gradients in austenite formed during UFH experiments, which defines the features of martensite-bainite aggregates and its fraction in the microstructure.

The initial microstructure strongly influences the properties after UFH. After all thermal cycles, the steels with microstructure ferrite and pearlite displayed higher ductility and lower strength than steels with 50% ferrite - 50% martensite initial microstructure.

It was found that, besides the tempering of martensite in the 50% M samples, the slow heating at 10 ^{o}C/s and holding at 300 °C for 30 s does not modify the overall texture nor the cementite morphology in F+P initial microstructure. This finding is important from a viewpoint of potential industrial application of the UFH because it gives more degree of freedom in the design of the heating devices.

6. Acknowledgements

The CONICYT-PCHA/Doctorado Nacional/2013 PhD scholarship for F. Castro Cerda is gratefully acknowledged. I. Sabirov acknowledges gratefully financial support via DIMMAT project funded by Madrid region under programme S2013/MIT-2775.

7. References

[1] R. Kuziak, R. Kawalla, S. Waengler, Advanced high strength steels for automotive industry, Arch. Civ. Mech. Eng. 8 (2014) 511. doi:10.1016/S1644-9665(12)60197-6.

[2] E. De Moor, P.J. Gibbs, J.G. Speer, D.K. Matlock, A.S. Processing, Strategies for Third-Generation Advanced High-Strength Steel Development, AIST Trans. 7 (2015) 2010.

[3] Q. Meng, J. Li, H. Zheng, High-efficiency fast-heating annealing of a cold-rolled dual-phase steel, Mater. Des. 58 (2014) 194–197. doi:10.1016/j.matdes.2014.01.055.

[4] D. De Knijf, A. Puype, C. Föjer, R. Petrov, The influence of ultra-fast annealing prior to

quenching and partitioning on the microstructure and mechanical properties, Mater. Sci. Eng. A. 627 (2015) 182–190. doi:10.1016/j.msea.2014.12.118.

[5] V. Massardier, A. Ngansop, D. Fabregue, S. Cazottes, J. Merlin, Ultra-Rapid Intercritical Annealing to Improve Deep Drawability of Low-Carbon, Al-Killed Steels, Metall. Mater. Trans. A. 43 (2012) 2225–2236. doi:10.1007/s11661-012-1096-6.

[6] R.H. Petrov, A. Puype, D. De Knijf, L. Kestens, Ultrafast heating of advanced high strength steels, in: and H.Z. Matthias Militzer, Gianluigi Botton, Long-Qing Chen, James Howe, Chadwick Sinclair (Ed.), Proc. Int. Conf. Solid-Solid Phase Transform. Inorg. Mater. 2015, 2015: pp. 1157–1158.

[7] T. Lolla, G. Cola, B. Narayanan, B. Alexandrov, S.S. Babu, Development of rapid heating and cooling (flash processing) process to produce advanced high strength steel microstructures, Mater. Sci. Technol. 27 (2011) 863–875. doi:10.1179/174328409x433813.

[8] D. Muljono, M. Ferry, D.P. Dunne, Influence of heating rate on anisothermal recrystallization in low and ultra-low carbon steels, Mater. Sci. Eng. A. 303 (2001) 90–99. doi:10.1016/S0921-5093(00)01882-7.

[9] R. Petrov, J. Sidor, W.J. Kaluba, L. Kestens, Grain Refinement of a Cold Rolled TRIP Assisted Steel after Ultra Short Annealing, Mater. Sci. Forum. 715-716 (2012) 661–666. doi:10.4028/www.scientific.net/MSF.715-716.661.

[10] F. Ramos, Ultra Fast Annealing of High-Strength Low-Alloy Steels (HSLAS), Ghent University, 2012.

[11] A. Puype, Developing of advanced high strength steel via ultrafast annealing, Ghent University, 2013. doi:10.1017/CBO9781107415324.004.

[12] R. Petrov, L. Kestens, W.J. Kaluba, Y. Houbaert, Recrystallization and austenite formation in a cold rolled TRIP steel during ultra fast heating, Steel Grips. 1 (2003) 289–293.

[13] P. Gobernado, R.H. Petrov, L.A.I. Kestens, Recrystallized {3 1 1}〈1 3 6〉 orientation in ferrite steels, Scr. Mater. 66 (2012) 623–626. doi:10.1016/j.scriptamat.2012.01.056.

[14] R.H. Petrov, J. Sidor, L.A.I. Kestens, Texture Formation in High Strength Low Alloy Steel Reheated with Ultrafast Heating Rates, Mater. Sci. Forum. 702-703 (2012) 798–801.

[15] V.T. G. Griffay, M. Anderhuber, P. Klinkenberg, New continuous annealing technology with high-speed induction heating followed by ultra-fast cooling, 2002.

[16] L. Kestens, A.C.C. Reis, W.J. Kaluba, Y. Houbaert, Grain Refinement and Texture Change in Interstitial Free Steels after Severe Rolling and Ultra-Short Annealing, Mater. Sci. Forum. 467-470 (2004) 287–292. doi:10.4028/www.scientific.net/MSF.467-470.287.

[17] T. Senuma, K. Kawasaki, Y. Takemoto, Recrystallization Behavior and Texture Formation of Rapidly Annealed Cold-Rolled Extralow Carbon Steel Sheets, Mater. Trans. 47 (2006) 1769–1775. doi:10.2320/matertrans.47.1769.

[18] Y.Y. Meshkov, E.V. Pereloma, Phase Transformations in Steels, Elsevier, 2012.

doi:10.1533/9780857096104.4.581.

[19] H.I. Aaronson, The proeutectoid ferrite and the proeutectoid cementite reactions, in: V.F. Zackay, H.I. Aaronson (Eds.), Decompos. Austenite by Diffus. Process., Metallurgical society of AIME, 1962.

[20] M. Hillert, ON THE THEORY OF NORMAL AND ABNORMAL GRAIN GROWTH, Acta Metall. 13 (1965) 227–238. doi:10.1017/CBO9781107415324.004.

[21] F.J. Humphreys, M. Hatherly, Recrystallization and Related Annealing Phenomena, Elsevier, 2004. doi:10.1016/B978-008044164-1/50018-9.

[22] M. Atkinson, Bifurcation of thermal restoration processes in deformed iron and steel, Mater. Sci. Eng. A. 262 (1999) 33–38. doi:10.1016/S0921-5093(98)01031-4.

[23] M. Atkinson, On the credibility of ultra rapid annealing, Mater. Sci. Eng. A. 354 (2003) 40–47. doi:10.1016/S0921-5093(02)00830-4.

[24] R.H. Goodenow, Recrystallization and grain structure in rimmed and aluminum killed low carbon steel, Trans. ASM. 59 (1966) 804–823.

[25] C.S. Smith, Grains, Phases, and Interfaces—an Interpretation of Microstructure, Trans. AIME. 175 (1948) 15–51.

[26] S.G. Chowdhury, E. V. Pereloma, D.B. Santos, Evolution of texture at the initial stages of continuous annealing of cold rolled dual-phase steel: Effect of heating rate, Mater. Sci. Eng. A. 480 (2008) 540–548. doi:10.1016/j.msea.2007.07.060.

[27] I. Samajdar, B. Verlinden, P. Van Houtte, D. Vanderschueren, γ-Fibre recrystallization texture in IF-steel: an investigation on the recrystallization mechanisms, Mater. Sci. Eng. A. 238 (1997) 343–350. doi:10.1016/S0921-5093(97)00455-3.

[28] J.Y. Kang, B. Bacroix, H. Réglé, K.H. Oh, H.C. Lee, Effect of deformation mode and grain orientation on misorientation development in a body-centered cubic steel, Acta Mater. 55 (2007) 4935–4946. doi:10.1016/j.actamat.2007.05.014.

[29] J.Y. Kang, D.I. Kim, H.C. Lee, Texture development in low carbon sheet steels for automotive application, in: A. Haldar, S. Suwas, D. Bhattacharjee (Eds.), Microstruct. Texture Steels Other Mater., Springer London, London, 2009: pp. 85–101. doi:10.1007/978-1-84882-454-6_5.

[30] R.K. Ray, J.J. Jonas, Transformation Textures in Steels, Int. Mater. Rev. 35 (1990) 1–36. <Go to ISI>://WOS:A1990DE71200001.

[31] M. Hillert, The growth of ferrite, bainite and martensite, in: J. Agren, Y. Brechet, C. Hutchinson, J. Philibert, G. Purdy (Eds.), Thermodyn. Phase Transform. Sel. Work. Mats Hillert, EDP Sciences, 2006: pp. 111–158.

[32] N.C. Law, D. V Edmonds, The formation of austenite in a low-alloy steel, Metall. Mater. Trans. A. 11 (1980) 33–46. doi:10.1007/BF02700436.

[33] M. Hillert, Phase Equilibria, Phase Diagrams and Phase Transformations: Their Thermodynamic Basis, Second ed, Cambridge University Press, New York, 2007.

[34] G.R. Speich, A. Szirmae, Formation of austenite from ferrite and ferrite-carbide aggregates, Trans. AIME. 245 (1969) 1063–1073.

[35] R.R. Judd, H.W. Paxton, Kinetics of austenite formation from a spheroidized ferrite-carbide aggregate, Trans. AIME. 242 (1968) 206–215.

[36] C.S. Roberts, Effect of carbon on the volume fractions and lattice parameters of retained austenite and martensite, Trans. AIME. 197 (1953) 203–204.

[37] W. Chen, K.C. Chan, P. Yu, G. Wang, Encapsulated Zr-based bulk metallic glass with large plasticity, Mater. Sci. Eng. A. 528 (2011) 2988–2994. doi:10.1016/j.msea.2010.12.077.

[38] W. Chen, J. Ketkaew, Z. Liu, R.M.O. Mota, K. O'Brien, C.S. da Silva, J. Schroers, Does the fracture toughness of bulk metallic glasses scatter?, Scr. Mater. 107 (2015) 1–4. doi:10.1016/j.scriptamat.2015.05.003.

[39] D. Xu, J. Li, Q. Meng, Y. Liu, P. Li, Effect of heating rate on microstructure and mechanical properties of TRIP-aided multiphase steel, J. Alloys Compd. 614 (2014) 94–101. doi:10.1016/j.jallcom.2014.06.075.

[40] J. Chiang, J.D. Boyd, A.K. Pilkey, Effect of microstructure on retained austenite stability and tensile behaviour in an aluminum-alloyed TRIP steel, Mater. Sci. Eng. A. 638 (2015) 132–142. doi:10.1016/j.msea.2015.03.069.

[41] Y.F. Shen, L.N. Qiu, X. Sun, L. Zuo, P.K. Liaw, D. Raabe, Effects of retained austenite volume fraction, morphology, and carbon content on strength and ductility of nanostructured TRIP-assisted steels, Mater. Sci. Eng. A. 636 (2015) 551–564. doi:10.1016/j.msea.2015.04.030.